A Fast Computational Technique for Accurate Permittivity Determination Using Transmission Line Methods

LEO P. LIGTHART

Abstract—**A fast analytical method is given for determining permittivity characteristics at microwave frequencies. The experimental setup uses a single-moded cylindrical waveguide filled with dielectric and followed by a load or by a moving short. In this way, transmission-reflection and short-circuited line methods are compared. By including the uncertainties in length and in the reflection and transmission parameters, the permittivity uncertainty region is determined. It is shown that for optimum accuracy of the permittivity, specific lengths in combination with a moving short are needed.**

I. Introduction

THE MOST ACCURATE determination of the permittivity of dielectrics at high frequencies can be obtained by using high Q resonant circuits. The main disadvantages of this method are that it can be applied only in a narrow frequency range, and that it is necessary to design the resonator. Permittivity measurements over a wide range of frequencies can be done, with reduced accuracy, when transmission line methods are used. A homogeneous dielectric with specific sample length is positioned in the terminated transmission line, and the permittivity can be derived from the measured transmission and reflection coefficient. In the case of finite measurement uncertainties, Stuchly and Matuszewski [1] found a considerable permittivity uncertainty. This uncertainty can be reduced by using the mutual relationship between the scattering coefficients. The method described here takes this relationship into account, and gives optimal results for a transmission line setup as found via the uncertainty analysis (Section III). The advantages of the present method are: a) the computation times required are small (a few milliseconds per permittivity uncertainty region); and b) the analytical expressions allow an optimization of the measurement configuration.

The disadvantages are: a) the limitation of small measurement uncertainty regions; and b) the complicated analysis.

This method is based on small measurement uncertainties and a single-moded cylindrical waveguide of specific length filled with dielectric and terminated with both a load and a moving short. For a set of frequencies, the scattering parameters at the waveguide reference planes are measured with sufficient accuracy by a slotted line, or by a calibrated network analyzer (type HP 8542B) at different positions of the moving short. For the use of the moving short in this measurement technique, one is referred to Deschamps [2]. The coupled scattering coefficients and their mutual uncertainties are calculated from these measurements. The computations for the scattering coefficients and the permittivity, including their uncertainties, can be performed within a negligible computing time by using the analytical expressions derived in Sections II and III.

It is claimed that this method is useful for accurate determination of the permittivity over a wide range of the frequency, the dielectric constant, and the loss factor. This permittivity measuring technique fills up the gap between the existing transmission-line and resonator-measuring techniques. Further, it allows a reconsideration of the existing methods in view of the possible known inaccuracies. The computer programs are simple and can be run on a 16-K minicomputer.

II. The Mutual Dependencies of the Scattering Coefficients and the Permittivity

In this section, we derive, under very strict model assumptions, two independent equations, both of which give the permittivity as a function of the two measured scattering coefficients. Starting from a given uncertainty limit of one of the scattering coefficients, we compute the accompanying scattering coefficient and vice versa. Only those scattering coefficients within uncertainty limits are used to compute the permittivity. For this purpose, the average values and the extreme variations of the scattering coefficients are selected.

Attention is given to model imperfections, and at the end of this section the measuring method with the moving short is shown to obtain the best measurement accuracy.

To derive the theory, the cross section of a cyclindrical single-moded waveguide is shown in Fig. 1 filled over a length l with a dielectric having unknown permittivity ϵ. The propagation constants are γ_0 in the empty waveguide and γ in the filled waveguide, and depend on the mode number m, the waveguide dimensions, the radian frequency ω, and the dielectric constant $n = \sqrt{\epsilon}$.

We know that

$$\gamma_0 = \sqrt{k_c^2 - k_0^2} \tag{1}$$

Manuscript received February 9, 1982; revised November 2, 1982.

The author is with the Delft University of Technology, Department of Electrical Engineering, Microwave Laboratory, P.O. Box 5031, Delft, the Netherlands.

0018-9480/83/0300-0249$01.00 ©1983 IEEE

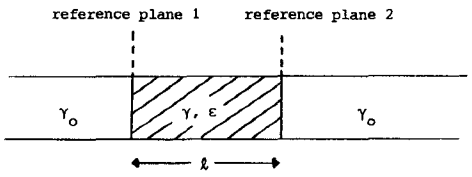

Fig. 1. Cross section of waveguide filled with dielectric.

where k_c = wave number at the cutoff frequency, depending on m and the waveguide dimension (e.g., $k_c = \pi/a$ for the TE_{01} mode where a = width of the waveguide and $k_c = 0$ for the TEM mode); and k_0 = wave number in free space = $\omega\sqrt{\epsilon_0\mu_0}$ where ϵ_0 and μ_0 are the permittivity and permeability in free space, respectively; and that

$$\gamma = \sqrt{k_c^2 - (nk_0)^2}\,. \tag{2}$$

The scattering matrix coefficients at the reference planes of this symmetrical two-port become [1]

$$S_{11} = S_{22} = -\rho(1-w^2)/(1-\rho^2 w^2) \tag{3}$$

$$S_{21} = S_{12} = w(1-\rho^2)/(1-\rho^2 w^2) \tag{4}$$

where

$$\rho = (\gamma/\gamma_0 - 1)/(\gamma/\gamma_0 + 1)$$

and

$$w = \exp(-\gamma l).$$

From (3) and (4), the reflection coefficient ρ and the propagation factor w can be derived as follows:

$$\rho = \frac{-\left(1+S_{11}^2 - S_1^2\right) + \sqrt{\left(1+S_{11}^2 - S_{21}^2\right)^2 - 4S_{11}^2}}{2S_{11}} \tag{5}$$

$$w = \frac{1 - S_{11}^2 + S_{21}^2 - \sqrt{\left(1 - S_{11}^2 + S_{21}^2\right)^2 - 4S_{21}^2}}{2S_{21}} \tag{6}$$

which means that

$$(\gamma/\gamma_0)^2 = \{(1-S_{11})^2 - S_{21}^2\}/\{(1+S_{11})^2 - S_{21}^2\} \tag{7}$$

$$v^2 = \{(1-S_{21})^2 - S_{11}^2\}/\{(1+S_{21})^2 - S_{11}^2\} \tag{8}$$

where $v = \mathrm{tgh}(\gamma l/2)$.

Equations (7) and (8) relate the propagation constant and the propagation factor to the scattering coefficients. To determine γ, we have two different equations, namely (7) and (8), in which γ is related to the scattering coefficients. With the exact scattering coefficients S_{11} and S_{21} and a given length l, we are able to compute the permittivity by using either (7) or (8). This means that by elimination of γ, a mutual dependency $h(S_{11}, S_{21})$ between S_{11} and S_{21} can be derived

$$h(S_{11}, S_{21}) = \frac{1 - S_{11}^2 + S_{21}^2}{S_{21}} - 2\cosh(\gamma l) = 0$$

$$\gamma l = \gamma_0 l \sqrt{\{(1-S_{11})^2 - S_{21}^2\}/\{(1+S_{11})^2 - S_{21}^2\}} \tag{9}$$

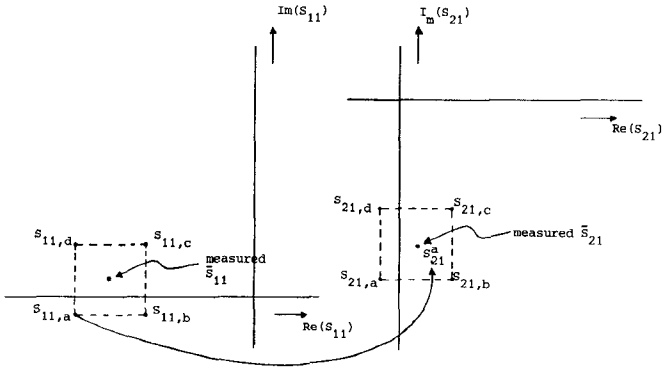

Fig. 2. Uncertainty regions around $\bar{S}_{11}$ and $\bar{S}_{21}$. $S_{11,a}$, $S_{11,b}$, $S_{11,c}$, and $S_{11,d}$ are the uncertainty limits for $\bar{S}_{11}$ and $S_{21,a}$, $S_{21,b}$, $S_{21,c}$, and $S_{21,d}$ for $\bar{S}_{21}$.

where the positive root can be taken in γl because in (9) only $\cosh(\gamma l)$ is present. Consequently, not only the measurement accuracy, but also the relationship just calculated between S_{11} and S_{21}, influences the uncertainties. This can be proved by analyzing the limits in the uncertainty regions which are due to measurement inaccuracies. The uncertainty limits $S_{11,a}$, $S_{11,b}$, $S_{11,c}$, and $S_{11,d}$ around the measured $\bar{S}_{11}$ and those of $S_{21,a}$, $S_{21,b}$, $S_{21,c}$, and $S_{21,d}$ around the measured $\bar{S}_{21}$ can be visualized as in Fig. 2. The different limits are substituted successively in (9) to compute the corresponding scattering coefficient. The procedure is as follows.

Starting from $S_{11} = S_{11,a}$, we compute the corresponding S_{21}^a by assuming (see Fig. 2)

$$S_{21}^a = \bar{S}_{21} + \delta_{21}^a \tag{10}$$

$$\gamma_{21}^a l = \gamma_0 l \sqrt{\{(1-S_{11,a})^2 - (\bar{S}_{21})^2\}/\{(1+S_{11,a})^2 - (\bar{S}_{21})^2\}}\,. \tag{11}$$

To find δ_{21}^a, we approximate (9) by the first terms of the Taylor expansion

$$0 = \left(1 + \delta_{21}^a \frac{\partial}{\partial \bar{S}_{21}}\right) \cdot h(S_{11,a}, \bar{S}_{21})$$

$$\delta_{21}^a = \frac{1 - (S_{11,a})^2 + (\bar{S}_{21})^2 - 2\bar{S}_{21}\cosh(\gamma_{21}^a l)}{-2\bar{S}_{21} + \dfrac{1-(S_{11,a})^2 + (\bar{S}_{21})^2}{\bar{S}_{21}} + 2\bar{S}_{21}\sinh(\gamma_{21}^a l)\dfrac{\partial(\gamma_{21}^a l)}{\partial \bar{S}_{21}}} \tag{12}$$

$$\frac{\partial(\gamma_{21}^a l)}{\partial \bar{S}_{21}} = -\gamma_{21}^a l \left\{ \frac{1}{(1-S_{11,a})^2 - (\bar{S}_{21})^2} - \frac{1}{(1+S_{11,a})^2 - (\bar{S}_{21})^2} \right\} \bar{S}_{21}. \tag{13}$$

We follow the same procedure for $S_{11} = S_{11,b}$, $S_{11,c}$, and $S_{11,d}$ to compute δ_{21}^b, δ_{21}^c, and δ_{21}^d, respectively, while for $S_{21} = S_{21,a}$, $S_{21,b}$, $S_{21,c}$, and $S_{21,d}$ we compute δ_{11}^a, δ_{11}^b, δ_{11}^c and δ_{11}^d, respectively, by a set of equations as listed below

for δ_{11}^a

$$S_{11,a} = \bar{S}_{11} + \delta_{11}^a \tag{14}$$

$$\gamma_{11}^a l = \gamma_0 l \sqrt{\left\{(1-\bar{S}_{11})^2 - (S_{21,a})^2\right\} / \left\{(1+\bar{S}_{11})^2 - (S_{21,a})^2\right\}} \tag{15}$$

$$\delta_{11}^a = \frac{1-(\bar{S}_{11})^2 + (S_{21,a})^2 - 2S_{21,a}\cosh(\gamma_{11}^a l)}{2\bar{S}_{11} + 2S_{21,a}\sinh(\gamma_{11}^a l)\dfrac{\partial(\gamma_{11}^a l)}{\partial \bar{S}_{11}}} \tag{16}$$

$$\frac{\partial(\gamma_{11}^a l)}{\delta \bar{S}_{11}} = -\gamma_{11}^a l \left\{ \frac{1-\bar{S}_{11}}{(1-\bar{S}_{11})^2 - (S_{21,a})^2} + \frac{1+\bar{S}_{11}}{(1+\bar{S}_{11})^2 - (S_{21,a})^2} \right\}. \tag{17}$$

To get a γ region solution, the S_{11} region determined by the four δ_{11} points needs an area in common with the uncertainty region of S_{11}, and can therefore be characterized by at least three points and maximally eight points. At the same time, the S_{21} region formed by the four δ_{21} points needs an area in common with the uncertainty region of S_{21} and can also be characterized by at least three points and maximally eight points. If the measurement accuracy is worse than specified, or the model assumptions are incorrect, it is possible that no common area is found, rendering an accurate determination of γ impossible. From the common area with minimally three and maximally eight extrema in S_{11}, the corresponding S_{21} values have to be found, and likewise with the extrema in S_{21}, the corresponding S_{11} values. These extrema are used to compute the average value S_{11}^{av} with corresponding $\tilde{S}_{21}$, and the average S_{21}^{av} with corresponding $\tilde{S}_{11}$. From the same data, the differences dS_{11}^{av}, $d\tilde{S}_{11}$, $d\tilde{S}_{21}$, and dS_{21}^{av} are derived as follows:

$$\begin{aligned} dS_{11}^{av} &= \text{extrema in } S_{11} \text{ within common } S_{11} \text{ area} - S_{11}^{av} \\ d\tilde{S}_{21} &= \text{corresponding } S_{21} - \tilde{S}_{21} \\ dS_{21}^{av} &= \text{extrema in } S_{21} \text{ within common } S_{21} \text{ area} - S_{21}^{av} \\ d\tilde{S}_{11} &= \text{corresponding } S_{11} - \tilde{S}_{11}. \end{aligned} \tag{18}$$

The combinations S_{11}^{av}, $\tilde{S}_{21}$, and $\tilde{S}_{11}$, S_{21}^{av} are used to compute γ twice by substituting these S parameters into (8). The differences in (18) are then used to compute the differences in γ according to the theory given in Section III. If the four areas formed by these differences in γ do not contain the difference in the two γ solutions, this indicates a nonlinearity in the method.

To study the model imperfections we distinguish: a) a length inaccuracy which can be taken into account as in Section III; b) a displacement of the reference planes, resulting in differences in the arguments of the measured $\bar{S}_{11}$ and $\bar{S}_{22}$ which can be taken into account by averaging these arguments; c) an air gap between the sample and the waveguide walls; d) the inhomogeneities within the sample; e) the excitation and propagation of higher order modes within the sample; and f) the nonplanar ends of the sample at the reference planes.

The last four model imperfections are taken into account by the enlargements of the uncertainty regions of $\bar{S}_{11}$ and/or $\bar{S}_{21}$ with the measured differences between $\bar{S}_{21}$ and $\bar{S}_{12}$, and between modulus ($\bar{S}_{11}$) and modulus ($\bar{S}_{22}$). It is clear that, for increased measurement accuracy, the common S_{11} and S_{21} areas become smaller so that stronger model conditions have to be fulfilled. The measurement accuracy in S_{11} and S_{21}, when measured as transmission and reflection coefficients with the HP 8542 B calibrated network analyzer, is sufficient for rather lossy materials if only (7) is used [1]. For low-loss materials with optimum results, the approach formulated in (7)–(18) has to be used. Examples of experimental results obtained with a waveguide slotted line and with the calibrated network analyzer are given in Section IV.

The random errors in the measurements are reduced with the reflection coefficient measurement method as described by Deschamps [2]. The method uses a load and a moving short behind the sample of Fig. 1 and was originally used for permittivity measurements by Altschuler [3].

When accurate scattering coefficient measurements of S_{11}, S_{22}, S_{21}, and S_{12} are desired, eight or even sixteen short-circuit positions spaced over half a wavelength can be used. The appeal of this method over the transmission and reflection method is that the mutual dependencies between the scattering coefficients are implicitly taken into account. For the calculation of the scattering coefficients, one is referred to [2].

III. The Optimal Measurement Configuration for Computing the Permittivity

In Section II, we have proved that there exists a mutual dependency between S_{11} and S_{21}. If we assume that S_{21} is a function of S_{11}, the error $d\epsilon_{11}$ in ϵ due to a sample length difference δl and to a difference dS_{11} (this can be dS_{11}^{av} or $d\tilde{S}_{11}$) becomes

$$d\epsilon_{11} = \frac{\partial \epsilon}{\partial l} \cdot \delta l + \frac{\partial \epsilon}{\partial S_{11}} \cdot dS_{11}, \qquad \text{for } \epsilon = \epsilon(S_{11}, l) \tag{19}$$

and for S_{11} as a function of S_{21}

$$d\epsilon_{21} = \frac{\partial \epsilon}{\partial l} \cdot \delta l + \frac{\partial \epsilon}{\partial S_{21}} \cdot dS_{21}, \qquad \text{for } \epsilon = \epsilon(S_{21}, l). \tag{20}$$

By using (1)–(4), (6), (7), and (9) we derive

$$\frac{\partial \epsilon}{\partial l} = \frac{2}{l}\left(\frac{\gamma}{k_0}\right)^2 \tag{21}$$

$$\frac{\partial \epsilon}{\partial S_{11}} = 4\left(\frac{\gamma}{k_0}\right)^2 \frac{1}{1-\rho^2} \frac{(1-\rho^2 w^2)^2}{4\rho w^2 \gamma l + (1+\rho^2 w^2)(1-w^2)} \tag{22}$$

$$\frac{\partial \epsilon}{\partial S_{21}} = \frac{2}{w}\left(\frac{\gamma}{k_0}\right)^2 \frac{1}{1-\rho^2} \frac{(1-\rho^2 w^2)^2}{\rho(1-w^2) + (1+\rho^2 w^2)\gamma l}. \tag{23}$$

From (21) we see that for length uncertainties

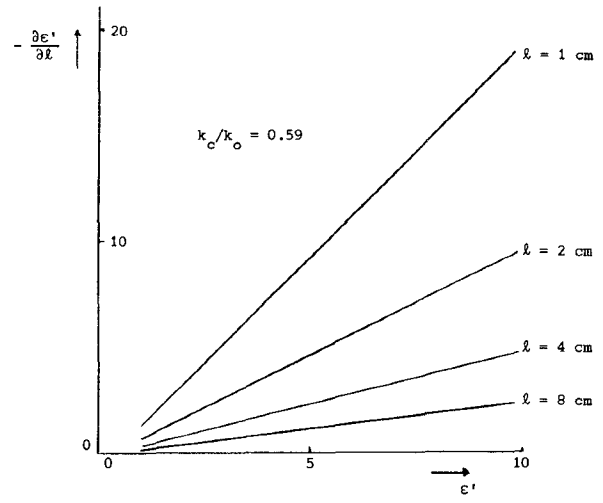

Fig. 3. The real part of (21) as a function of ϵ' for different lengths and $k_c/k_0 = 0.59$.

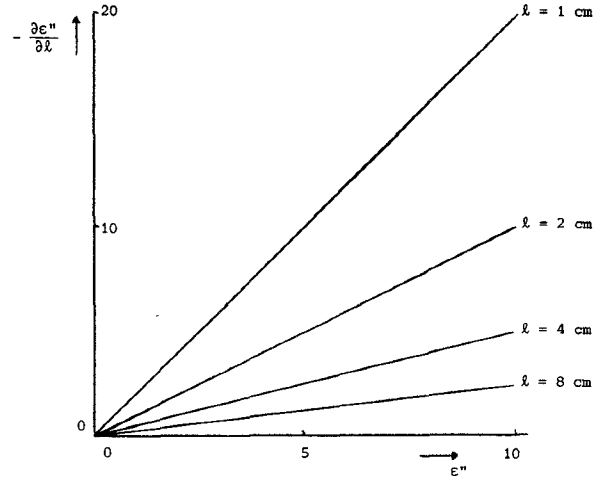

Fig. 4. The imaginary part of (21) as a function of ϵ'' for different lengths.

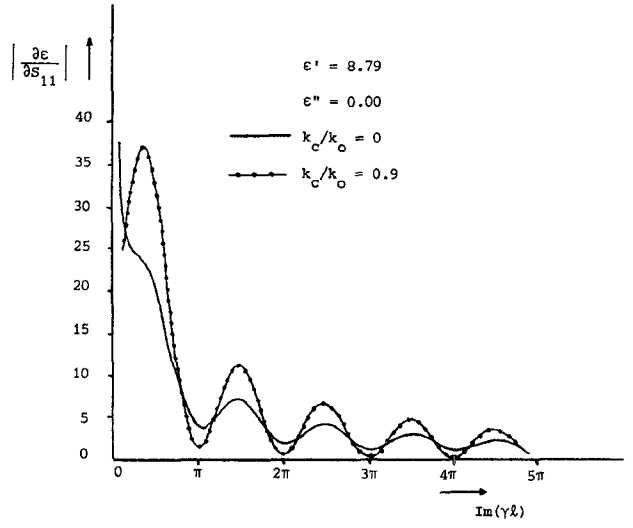

Fig. 5. The modulus of (22) as a function of $\mathrm{Im}(\gamma l)$ for different k_c/k_0.

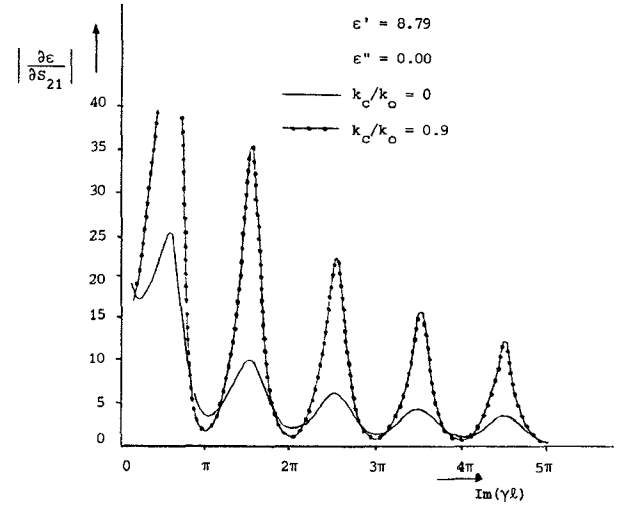

Fig. 6. The modulus of (23) as a function of $\mathrm{Im}(\gamma l)$ for different k_c/k_0.

$\mathrm{Re}(\partial\epsilon/\partial l)$ = real part of $\partial\epsilon/\partial l$ depends on $\mathrm{Re}(\epsilon) = \epsilon'$ and becomes minimal for maximum length and for measurement wavelengths near cutoff. $\mathrm{Im}(\partial\epsilon/\partial l)$ = imaginary part of $\partial\epsilon/\partial l$ is a function of $\mathrm{Im}(\epsilon) = \epsilon''$, and becomes minimal for maximum length, but does not depend on the empty transmission line cutoff wavelength. For that reason, the real and imaginary parts of (21) are shown in Figs. 3 and 4.

To analyze the influences of scattering coefficient uncertainties for different sample lengths, first the limitation of dielectric materials without losses is considered. This means

$$\epsilon'' = 0 \Rightarrow \mathrm{Im}(\rho) = \mathrm{Re}(\gamma) = 0. \tag{24}$$

In that case, the absolute values of (22) and (23) have been visualized in Figs. 5 and 6, e.g., for $\epsilon' = 8.79$. The reason why we take the absolute values is because dS_{11} and dS_{21} have complex values around S_{11}^{av} with corresponding $\tilde{S}_{21}$, or around S_{21}^{av} with corresponding $\tilde{S}_{11}$. Contrary to the length uncertainty, we therefore assume equal influences on $d\epsilon'$ and $d\epsilon''$ due to uncertainties in dS_{11} and dS_{21}. From Figs. 5 and 6, we conclude that for optimum computation of the permittivity, ρ has to be as large as possible and

$$\mathrm{Im}(\gamma l) = k\pi, \qquad k = 0, 1, 2 \cdots \tag{25}$$

where larger k gives more accurate ϵ' values but at the same time implies more stringent considerations concerning the model assumptions. Increasing ρ can be reached by using the empty waveguide near cutoff. The most attractive feature of the method with the automatic network analyzer, however, is broad-bandedness. This means that the near cutoff waveguide option would not be generally available.

A second advantage of the sample lengths given by (25) is that for this idealized case $|S_{11}|$ becomes 0. This means that $|dS_{11}|$, and also $|dS_{21}|$, because of the mutual dependency between S_{11} and S_{21}, become minimal.

If losses are taken into account, $\epsilon'' \neq 0$, and so $\mathrm{Re}(\gamma) = \alpha \neq 0$. Because $|S_{11}| \neq 0$, and thus $|dS_{11}|$ increases when compared to the lossless case, the permittivity results become less accurate for optimum sample lengths given by (25).

From (22) and (23) we see that for lossy materials the S_{21} measurements largely determine the accuracy in the permittivity results for sample lengths very large in relation to the wavelength because only the minima of (23) and $|S_{21}|$ decrease with increasing sample length. This is in agreement with [4], where the influence of the sample length for high ε' ferroelectric materials in a TE measurement config-

uration has been studied by using the amplitude and phase of S_{21} only. For an arbitrary sample length, both (22) and (23) have to be used to achieve the most accurate results.

IV. Results

Firstly, we show the influence on the accuracy of $\epsilon = \epsilon' + j\epsilon''$ measurements at frequencies near the cutoff frequency of the empty waveguide. We take the example of the TE_{01} mode propagating in a rectangular waveguide (inner dimensions 25.8 mm × 51.6 mm), and homogeneously filled over a length $L = 8.92$ mm with aluminum oxide corresponding to a quarter wavelength inside this medium at a frequency of 3 GHz. The scattering coefficients $\bar{S}_{11}$ and $\bar{S}_{21}$ and the uncertainty limits as suggested by the manufacturer of the HP calibrated network analyzer type HP 8542 B become

$$f = 3 \text{ GHz}, \quad \text{length} = 8.92 \text{ mm} \pm 0 \text{ mm}$$
$$\text{Re}(S_{11}) = -0.983 \pm 0.030, \quad \text{Im}(S_{11}) = 0 \pm 0.030$$
$$|S_{21}| = 0.177 \pm 0.003, \quad \arg(S_{21}) = -1.57 \pm 0.040.$$

The uncertainty limits are checked by turning the sample so that S_{22} and S_{12} are measured, and further by computing δ_{21} ((12)), under the assumption of an infinitesimal uncertainty region of S_{11}, and by computing δ_{11} ((16)), under the assumption of an infinitesimal uncertainty region of S_{21}. If the differences between $\bar{S}_{11}$ and $\bar{S}_{22}$ or between $\bar{S}_{21}$ and $\bar{S}_{12}$, or if δ_{21} or δ_{11} are larger than the HP uncertainty limits due to incorrect model considerations, including length uncertainties, the uncertainty region has to be enlarged. By using (10)–(17), and (1), (2), and (18)–(23), the common ϵ area has been calculated. In Fig. 7 the common ϵ area has been drawn with solid lines; for comparison, the broken lines indicate the common ϵ area as obtained in a TEM configuration with the same electrical length of the sample.

For a sample length of 17.83 mm, corresponding to the optimum electrical length of half a wavelength, the scattering coefficients with their uncertainties become

$$f = 3 \text{ GHz}, \quad \text{length} = 17.83 \text{ mm} \pm 0 \text{ mm}$$
$$\text{Re}(S_{11}) = -0.089 \pm 0.003, \quad \text{Im}(S_{11}) = 0.001 \pm 0.003$$
$$|S_{21}| = 0.91 \pm 0.017, \quad \arg(S_{21}) = 3.142 \pm 0.027.$$

For this optimum length, the common ϵ area is shown in Fig. 8 for the TE_{01} mode and is compared to the TEM mode.

From Figs. 7 and 8, we see the advantage of using the TE_{01} mode near cutoff for sample lengths which satisfy (25).

The method with the moving short has been used for the ϵ determination of plexiglass in the case of nonoptimum sample length. From sixteen measurements with the moving short, and one S_{11} measurement with a load, we have derived from Deschamps [2] the scattering coefficients with their uncertainties for

$$f = 9.814 \text{ GHz}, \quad \text{length} = 74.5 \text{ mm} \pm 0 \text{ mm}.$$
$$\text{Re}(S_{11}) = -0.142 \pm 0.019, \quad \text{Im}(S_{11}) = -0.186 \pm 0.019$$
$$|S_{21}| = 0.881 \pm 0.021, \quad \arg(S_{21}) = 2.696 \pm 0.031.$$

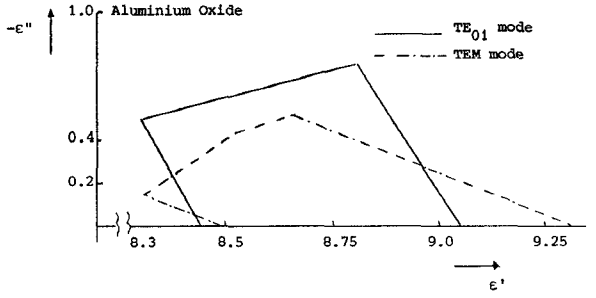

Fig. 7. Uncertainty limits of ϵ, predicted from uncertainty limits of S_{11} and S_{21}, as obtained for a quarter-wave sample in a TEM transmission line and a TE_{01} waveguide near cutoff. (The lower boundary of ϵ'' has not been shown because it corresponds with active materials.)

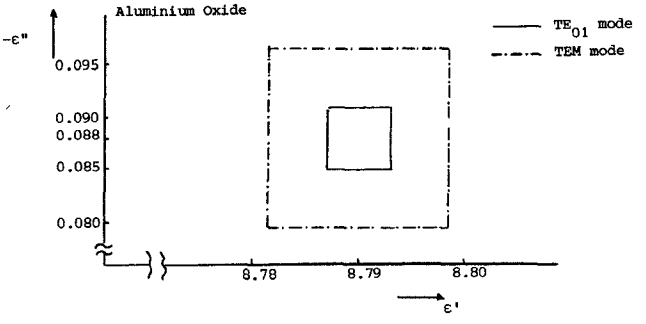

Fig. 8. Uncertainty limits of ϵ, predicted from uncertainty limits of S_{11} and S_{21}, as obtained for half a wavelength sample in a TEM transmission line and a TE_{01} waveguide near cutoff.

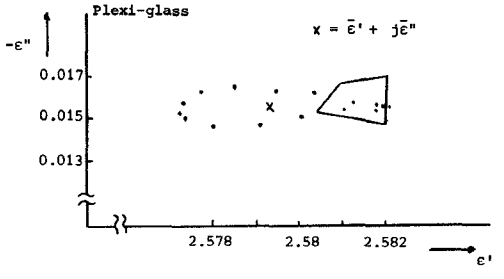

Fig. 9. Uncertainty limits of ϵ predicted from computed uncertainty limits of S_{11}, S_{21} (solid lines) [2], and sixteen computed S_{11}, S_{21} values (dots).

The results (solid lines) are given in Fig. 9.

If we use the sixteen measurements separately to compute S_{21} via

$$S_{21}^2 = \frac{(\Gamma_k' - S_{11})(1 - S_{11}\Gamma_k)}{\Gamma_k}$$

where Γ_k = complex reflection coefficient of the moving short at the output reference plane, and Γ_k' = measured reflection coefficient at the input reference plane, we are able to compute sixteen different ϵ's ((8)), indicated by dots in Fig. 9, resulting in

$\bar{\epsilon}'$ = average in $\epsilon' = 2.5793$, $S_{\epsilon'}$ = spread in $\epsilon' = 0.0020$

$\bar{\epsilon}''$ = average in $\epsilon'' = -0.0156$, $S_{\epsilon''}$ = spread in $\epsilon'' = 0.0006$.

Comparison between the dots and the common ϵ area in Fig. 9 indicates an accuracy in ϵ' and ϵ'' better than 0.001. The fact that the dots follow a smooth contour rather than scatter randomly suggests that there is some systematic

error in S_{11} and S_{21}. Minimizing the area of the contour by varying S_{11} within the uncertainty limits can further improve the ϵ accuracy.

V. Conclusions

The analytical approach to computing ϵ from reflection and/or transmission coefficients as derived in Section II has the advantage that the programming is simple and can be performed within a negligible computing time in the minicomputer which is part of the automatic and calibrated network analyzer. In Section III, the ϵ uncertainty region is related to the sample length uncertainty, and to the scattering coefficient uncertainties. For low-loss materials, accurate ϵ results are obtained by measuring S_{11} for long sample lengths corresponding to an integer number times half a wavelength in the medium, especially when a rectangular waveguide near cutoff is used. However, the longer the sample lengths are, the more sensitive the ϵ computations are to failures in the model. For higher losses, the influence of S_{21} becomes more important and both minima of (22) and (23) have to be used to get the most accurate results. Under the assumption of sufficient measurement sensitivity, the method with the moving short has the advantage that only reflection coefficients have to be measured. From these measurements, the scattering coefficients and their uncertainties are derived. A variant makes use of the relation between the scattering coefficients via the measured reflection coefficients. The different ϵ results found in this manner yield comparable results and can be analyzed statistically.

Acknowledgment

Thanks are due to M. K. Smit, who thoroughly discussed this subject with me, and to M. de Kok, who did the measurements with and the programming for the automatic and calibrated network analyzer.

References

[1] S. S. Stuchly and M. Matuszewski, "A combined total reflection-transmission method in application to dielectric spectroscopy," *IEEE Trans. Instrum. Meas.*, vol. IM-27, no. 3, pp. 285–288, Sept. 1978.

[2] G. A. Deschamps, "Determination of reflection coefficients and insertion loss of a waveguide junction," *J. of Appl. Phys.*, vol. 24, no. 8, pp. 1046–1051, Aug. 1953.

[3] H. M. Altschuler, *Handbook of Microwave Measurements*, M. Sucher and J. Fox, Eds. vol. 2. New York: Wiley, section 9.08, 1963.

[4] J. B. Horton and G. A. Burdick, "Measurement of dielectric constant and loss tangent in materials having large dielectric constants," *IEEE Trans. Microwave Theory Tech.*, vol. MTT-16, pp. 873–875, Oct. 1968.

Leo P. Ligthart was born in Rotterdam, The Netherlands, on September 15, 1946. He graduated with distinction in 1969 and received the M.S. degree in electrical engineering from Delft University of Technology.

Since 1969 he has been with the Microwave Laboratory of the Delft University of Technology. In 1974 he became Senior Lecturer teaching undergraduate courses in Transmission Line Theory, Antennas, and Propagation. During the 1976–1977 academic year he was on leave at the Chalmers University of Technology, Gothenborg, Sweden. Since 1977 he has been a Senior Staff Engineer working on antennas and tropospheric radar.